Pure Appl. Geophys. 175 (2018), 793–811

https://doi.org/10.1007/s00024-017-1709-5

Pure and Applied Geophysics

Seismic Parameters of Mining-Induced Aftershock Sequences for Re-entry Protocol Development

Javier A. Vallejos[1] and Rodrigo A. Estay[1,2]

Abstract—A common characteristic of deep mines in hard rock is induced seismicity. This results from stress changes and rock failure around mining excavations. Following large seismic events, there is an increase in the levels of seismicity, which gradually decay with time. Restricting access to areas of a mine for enough time to allow this decay of seismic events is the main approach in re-entry strategies. The statistical properties of aftershock sequences can be studied with three scaling relations: (1) Gutenberg–Richter frequency magnitude, (2) the modified Omori's law (MOL) for the temporal decay, and (3) Båth's law for the magnitude of the largest aftershock. In this paper, these three scaling relations, in addition to the stochastic Reasenberg–Jones model are applied to study the characteristic parameters of 11 large magnitude mining-induced aftershock sequences in four mines in Ontario, Canada. To provide guidelines for re-entry protocol development, the dependence of the scaling relation parameters on the magnitude of the main event are studied. Some relations between the parameters and the magnitude of the main event are found. Using these relationships and the scaling relations, a space–time–magnitude re-entry protocol is developed. These findings provide a first approximation to concise and well-justified guidelines for re-entry protocol development applicable to the range of mining conditions found in Ontario, Canada.

Key words: Mining seismicity, Omori's law, Båth's law, Reasenberg–Jones model, re-entry protocol, mine safety.

1. Introduction

Immediately following large seismic events/rock burst or blasts in seismically active mines, there is a short-term increase of the levels of seismicity that gradually decay to background levels. The complete phenomenon is known as an aftershock sequence. During this time of elevated seismicity, the risk of aftershocks with sufficiently high magnitude to cause damage increases. Therefore, the policy adopted by mines is to restrict access to the affected areas for a space–time period, known as exclusion zone. This is the re-entry protocol (Vallejos and McKinnon 2008, 2009a, b, 2010, 2011; Vallejos 2010).

The decay pattern follows the modified Omori's law (MOL) (Utsu et al. 1995) developed from observed decay rates of large earthquake aftershocks:

$$n(t) = \frac{K}{(c+t)^p}, \tag{1}$$

where $n(t)$ is the event rate since time t measured from the main event, c is a time offset constant, p controls the speed of decay and differs from sequence to sequence, with a typical range for tectonic earthquakes of 0.6–1.6 and a median value of 1.1 (Utsu et al. 1995), and K is an activity parameter related to the number of events within the sequence.

The power law form of Eq. (1) indicates that there is no characteristic time scale and, for large time ($t \gg c$), the equation is temporally self-similar (Ito and Matsuzaki 1990). However, when the MOL curvature is traced in time, a characteristic point emerges at the maximum curvature, given by

$$T_{\mathrm{MC}} = \left[Kp\sqrt{\frac{2p+1}{p+2}} \right]^{\frac{1}{1+p}} - c, \tag{2}$$

T_{MC} is the maximum curvature's time and it has a physical attribute of a time sequence that obeys MOL decay, suitable for use in re-entry protocols, defining the transition between the highest to lowest event rate change (Vallejos and McKinnon 2010).

Previous studies (Vallejos and McKinnon 2008, 2009a, b, 2010, 2011; Vallejos 2010) have established guidelines for re-entry protocol

[1] Advanced Mining Technology Center (AMTC), Department of Mining Engineering, University of Chile, Av. Tupper 2069, 837-0451 Santiago, Chile. E-mail: javallej@ing.uchile.cl

[2] *Present Address*: Department of Metallurgical and Materials Engineering, Federico Santa María Technical University, Av. España, 1680 Valparaiso, Chile.

development based on an analysis of current re-entry practices in Ontario's mines, and a statistical analysis of the MOL's decay parameters. In addition, correlations between certain mining factors such as volume of mined rock, the depth and the magnitude of large events (Vallejos and McKinnon 2011) and seismicity have been proposed.

The main goal of this paper is to explore correlations between the seismic parameters of mining-induced seismicity and the magnitude of the main event, to be applied in re-entry protocols. To accomplish this, three scaling relations are studied: (1) Gutenberg–Richter frequency magnitude (Richter 1958), (2) the modified Omori's law (MOL) for the temporal decay (Utsu et al. 1995), and (3) Båth's law for the magnitude of the largest aftershock (Båth 1965). The Reasenberg–Jones stochastic model (Reasenberg and Jones 1989, 1994) is also included in the analysis. The aftershock sequence patterns described by these scaling laws and their implications for re-entry assessment are addressed and discussed. Using the scaling relations, a space–time–magnitude re-entry protocol is developed applicable to the range of mining conditions found in Ontario, Canada.

2. Sources of Data and Aftershock Sequences

Seismic data from the following four mining operations in Ontario, Canada, are used throughout this paper, including

1. Copper Cliff North, Sudbury.
2. Craig, Sudbury.
3. Creighton, Sudbury.
4. Kidd Creek, Timmins.

Each mine has a monitoring system provided by the Engineering Seismology Group (ESG) Company, ensuring that the hypocentres location and the calculation of magnitudes are consistent. The wide variety of mining and geology is selected to evaluate the range of aftershock statistics that can be found in mining operations in Ontario.

In the following, an overview of the geology and monitoring systems of each mining site is provided.

2.1. Geology and Monitoring System

Each mine, except Kidd Creek, is located around the Sudbury Igneous Complex (SIC) (Fig. 1), which corresponds to a 2.5–3.0 km thick with $\sim 60 \times 27$ km elliptical igneous rock body (Therriault et al. 2002). The geology of the Sudbury Igneous Complex is described in Fig. 2.

1. *Copper Cliff North, Sudbury* It is located at N46°26.930′, W81°05.725′. The study area consists on the upper part of the 100/900 orebodies, between the 2700 and 3400 levels. The microseismic monitoring system covering this zone is made up by 13 uniaxial and two triaxial accelerometers. Various mining methods have been used over the years at North Mine, but the

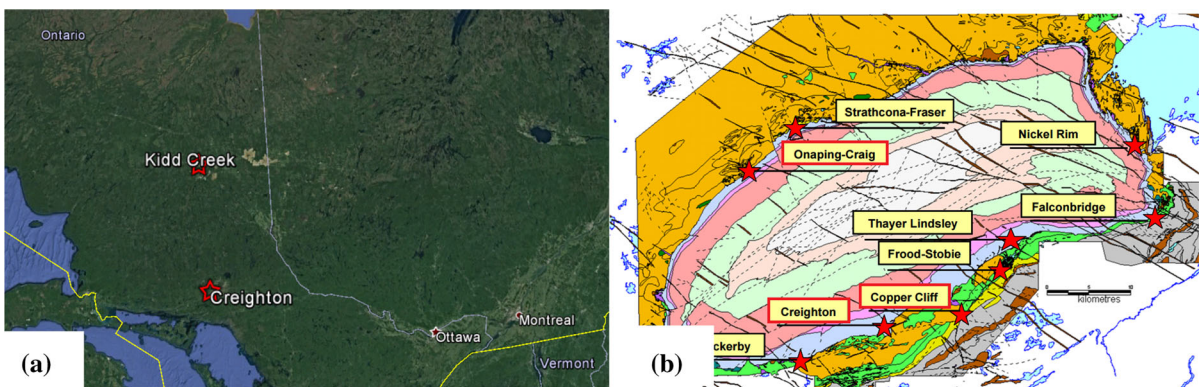

Figure 1
a Location of Kidd Creek and Creighton Mine, which indicates the location of the Sudbury Igneous Complex. **b** Location of the mines around the Sudbury Igneous Complex. The names of the mines framed with a red rectangle are those used in this study. Modified from Villaescusa et al. (2007)

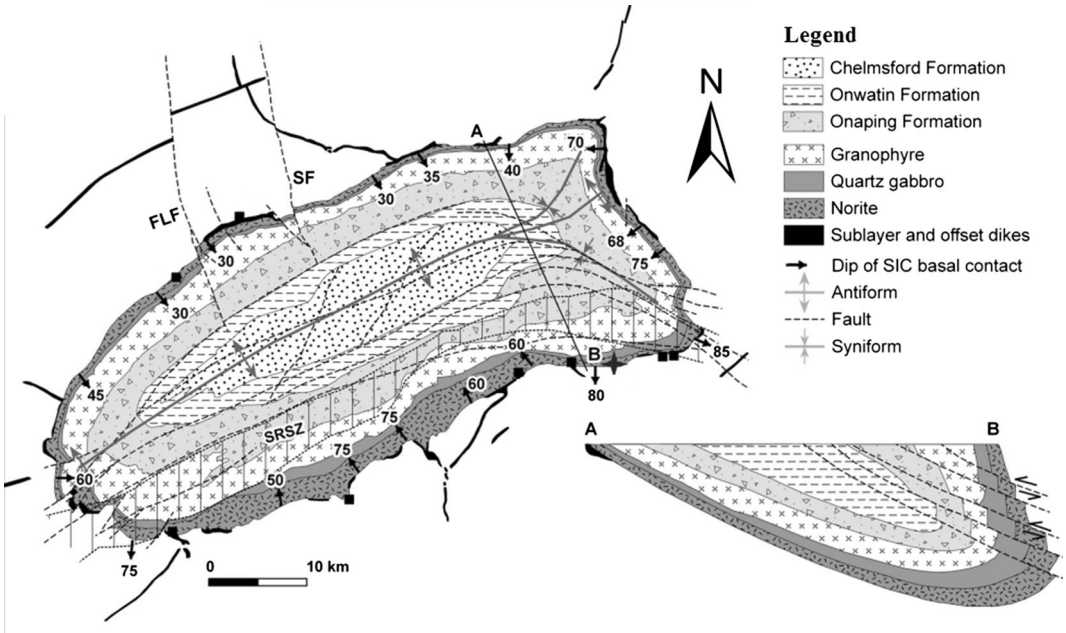

Figure 2
Geology of the Sudbury Igneous Complex. *FLF* Fecunis Lake Fault, *SF* Sandcherry Fault, *SRSZ* South Range Shear Zone. Modified from Mukwakwami et al. (2011)

main methods used presently are slot/slash and vertical retreat mining in the main mining block of the mine. The ore deposits of the North Mine environment predominantly occur within the intrusive quartz diorite dyke (Fig. 3). The quartz diorite dyke striking north–south is approximately 50 m wide and generally dips vertically or steeply to the west. The nickel–copper sulphides are generally located in the central portion of the quartz diorite dyke, and form elongated steeply plunging pipe-like orebodies. The country rocks west of the dyke are predominantly granite and granodiorite rocks of the Creighton Pluton. The country rock, east of the dyke, is made up by metavolcanic and metasedimentary rocks of the Elsie Mountain Formation. Sudbury Breccia predominantly occurs east of the dyke and is widespread at breaks in the dyke. Narrow quartz diabase and olivine diabase dykes crosscut the quartz diorite dyke. The North Mine is associated with four major faults: number 2 mine fault, number 1 cross fault, 900 Orebody Cross fault and Creighton fault at the south end of the North Mine. The faulting was the last geological event affecting the North Mine environment; it displaced the quartz diorite dyke and its associated ore deposits, the quartz diabase dykes, and the olivine diabase dykes.

2. *Craig Mine, Sudbury* Craig Mine is a nickel–copper deposit located on the Northwest rim of the Sudbury Basin (N46°38.1′, W81°22.2′). These zones of the Craig Mine have a fault region obliquely traversing the orebody generating high seismic activity and occasional large magnitude events. These zones are currently being mined via blast hole open stoping. The seismic array has 55 uniaxial sensors and covers a volume of approximately 1000 × 1300 × 900 m.
3. *Creighton Mine, Creighton* Creighton Mine is located within the Creighton embayment on the outer rim of the South Range of the Sudbury Igneous Complex (N46°27.7′, W81°11.4′). At depth, the Creighton main ore zone strikes roughly east–west and dips steeply to the north. Creighton Mine comprises 15 orebodies of which most of the higher grade mineralization has been depleted. Mineralization is contained within a northwest plunging embayment of norite in the footwall.

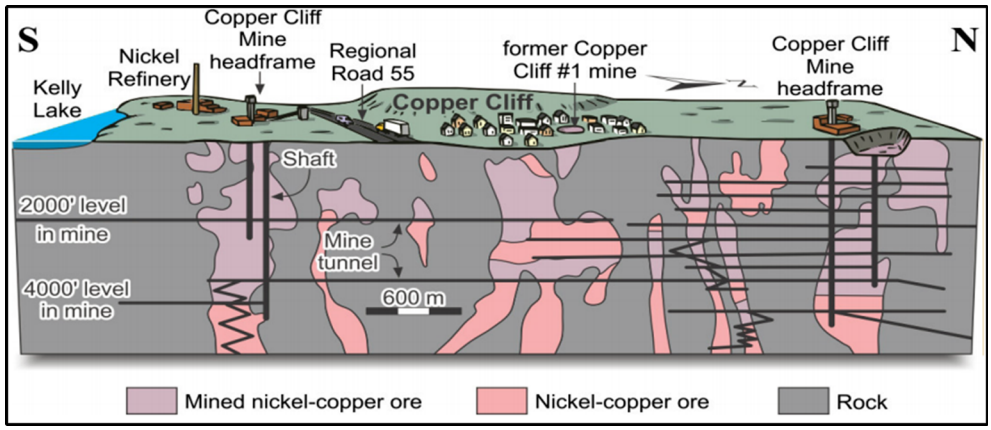

Figure 3
A cross-section of the underground workings of the Copper Cliff Mine, looking west. From Natural Resources Canada and Ontario Geological Survey (2015)

Creighton Mine is characterized by several late-stage faults, locally termed shears. The structures consist of foliated material. Depending on the structure, shear zones vary in thickness from a few centimetres to tens of meters (Malek et al. 2009). The study region corresponds to the Creighton Deep, between the 6600 and 7800 levels (between 1828 and 2377 m below the surface) (Fig. 4). The underground microseismic monitoring system covering this area consists of 24 uniaxial and seven triaxial accelerometers.

4. *Kidd Creek*, *Timmins* Kidd Creek Mine is located 24 km north from Timmins, Ontario (N48°41′, W81°22.3′) The study region corresponds to the complete mine D, covering a volume of approximately 300 × 9200 × 9500 m, between the 6800 and 8800 levels (between 2073 and 2682 m below the surface) (Fig. 5a). In this zone, the underground microseismic monitoring system consists of 15 uniaxial and four triaxial accelerometers. Blast hole mining with delayed paste backfill is used to mine the ore underground. A general description of the mine's geology can be found in Board et al. (2001). Kidd Mine's main mineralized lenses are called the main (copper stringer and massive sulphides) and south lenses. These orebodies are located near the top of a locally thickened rhyolite, which is underlain to the east by ultramafics and overlain to the west by mafic flows and associated intrusions. The stratigraphy trends north–south is overturned, and dips steeply to the east. All the lithologies in the Kidd Mine (Fig. 5b), including the ore have been subjected to complex folding and faulting. The major faults that potentially affect the mine-wide stability can be defined in two systems: the Gouge Fault and the south-dipping echelon faults. The south-dipping faults have been associated with the larger seismic events at Kidd, while the Gouge Fault and its splays primarily impact the hanging wall dilution.

2.2. *Aftershock Sequences*

Several aftershock sequences have been collected from several mine-wide large magnitude events at different sites in Ontario, Canada (Table 1).

The main shock magnitude was given in the Nuttli magnitude scale (M_n) (Nuttli 1973) that is used to express the magnitude of large seismic events for mines in the Canadian Shield. All the aftershocks in the sequences were measured in moment magnitude scale. Because of that and to ensure the correct estimation of the seismic parameters, the Nuttli magnitude will be converted into moment magnitude ($M_{w,m}$) through the following relation:

$$M_{w,m} = 1.03M_n - 0.61. \quad (3)$$

Sonley and Atkinson (2005) found these empirical relationships between M_n and $M_{w,m}$, using small

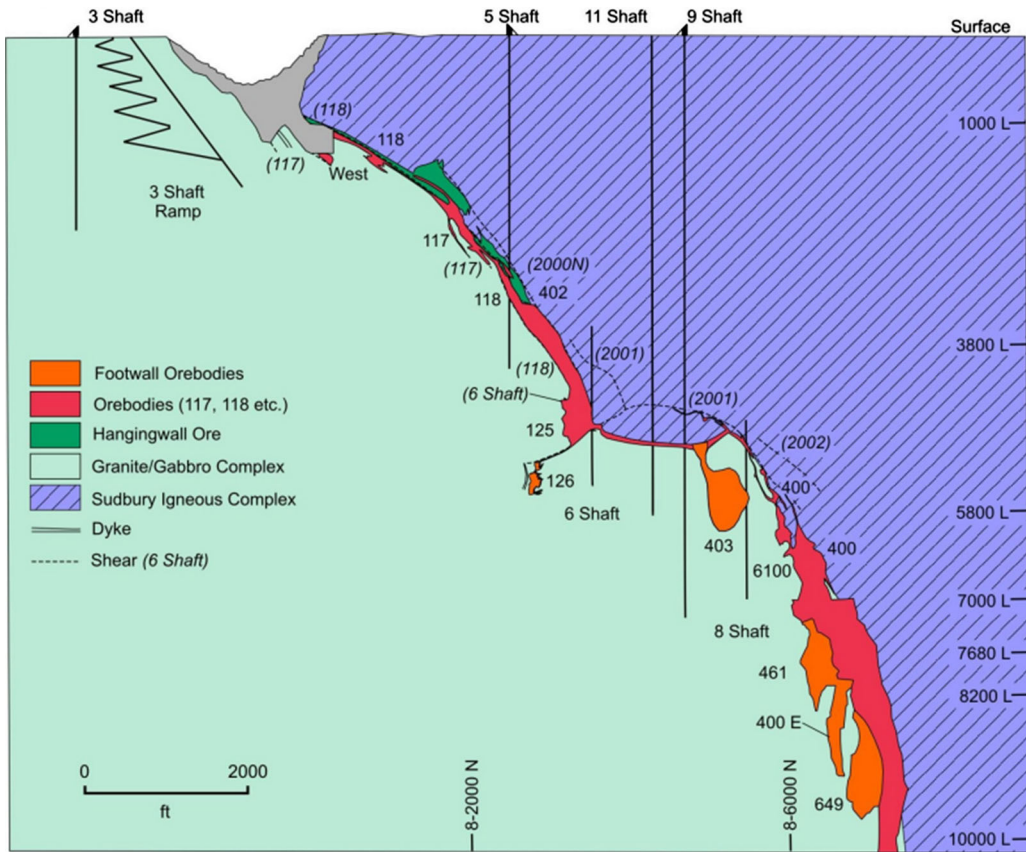

Figure 4
Cross-section of the Creighton Mine. From Malek et al. (2009)

earthquakes in Brunswick Mine (Canada) with $1.0 \leq M_{\mathrm{n}} \leq 6.0$.

The total duration of the sequence (t_N) was estimated by ratios method, described by Frohlich and Davis (1985) and following the considerations of Vallejos and McKinnon (2010). This method evaluates the ratio

$$r(N_b, N_a) = T_{N_a}/T_{N_b}, \tag{4}$$

where T_{N_a} and T_{N_b} are the time of occurrence of the N_ath and N_bth event following and preceding the principal event, respectively. Subsequent events are identified as aftershocks if the above ratio is smaller than a critical value generated by a random process with a certain probability. For our analysis, we set $N_a = 1$, $N_b = 5$ with a probability of 1%, giving a critical value of $r_{\mathrm{c}}(5,1) = 0.002$. The start of the sequence is defined if the ratio $r(5,1)$ is less than the critical value for a group of at least three consecutive events.

3. Methodology

Figure 6 presents a flowchart of the methodology applied in this paper that combines filtering, clustering tools and estimation of seismic parameters of the three scaling relations: Omori's law, Gutenberg–Richter law and Båth's law. The implications of these scaling relations for re-entry protocol development are presented as the outcome of the analysis.

3.1. Aftershock Sequence Filtering

Each aftershock sequence was filtered by limiting the source location error (Δr), and by magnitude of

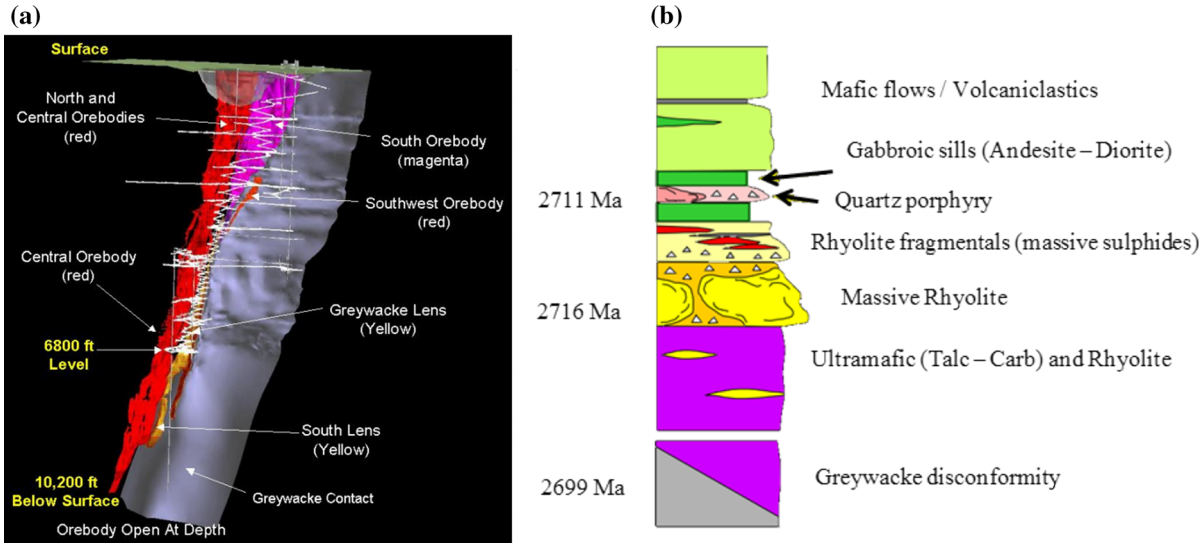

Figure 5
a Kidd Creek Mine ore bodies looking East from the surface to 3110 m (10,200 ft). **b** Stratigraphy and lithology in Kidd Creek Mine (Gibson et al. 2003)

completeness ($M_{w,c}$). The objective of these two constraints is to remove the poorly located seismic events from the analysis and to provide some degree of uniformity to the data. For the analysis, only seismic events with an associated hypocentral location error less than or equal to 50 m were considered. This distance matches with the minimum spherical radius used to restrict access from the potential source after a large magnitude event (Vallejos and McKinnon 2008).

The $M_{w,c}$ value for each sequence was estimated by the Goodness of Fit (GoF) method (Wiemer and Wyss 2000). In the GoF method, a minimum adjustment of $R_{GoF} = 90\%$ between the observed and predicted cumulative number of events was considered. The same procedure explained by Wiemer and Wyss (2000) is applied.

To select a single $M_{w,c}$ value represented by $M^*_{w,c}$ for the analysis, the following methodology is applied:

1. A tentative $M^*_{w,c}$ value is selected.
2. Aftershock sequences that satisfy $M_{w,c} \leq M^*_{w,c}$ are considered for the analysis.
3. Next, the procedure presented in Fig. 6 is applied, considering only the pre-processing (filtering and clustering) and the estimation of seismic parameters of the Gutenberg–Richter and the modified Omori's law. Only sequences with more than ten events are considered for the analysis. The correlations between the seismic parameters and the magnitude of the main shock are estimated.
4. The selected $M^*_{w,c}$ is the minimum value which maximizes the correlation between the seismic parameter and the main shock magnitude, and it is greater than the maximum $M_{w,c}$ value of all the sequences (in this case − 1.4, Table 2).

Based on the above procedure, a value of $M^*_{w,c} = -1.30$ was determined.

3.2. Spatial Clustering

The sequences presented in Table 1 only consider the end time of the sequence, independent of the spatial distribution of the seismicity. To ensure that only the main group of seismicity associated in space to the large magnitude event is included into the sequence, a single-link, or nearest neighbour cluster method was applied to each aftershock sequence. This type of hierarchical cluster method is one of the oldest methods of cluster analysis (McQuitty 1957; Sneath 1957) and it has been used to evaluate clustering in numerous fields (Ling 1973; Hartigan 1975; Day and Edelsbrunner 1984; Frohlich and Davis 1990; Davis and Frohlich 1991a; b; Dieterich

Table 1

List of analysed aftershock sequences (Seq) following large magnitude events collected from Ontario mines, Canada

Seq	Site	Date (mm/dd/yyyy)	M_n	$M_{w,m}$	t_N (h)	Number of events	
						Pre clustering	Post clustering
1	CCN	06/10/2005	2.1	1.6	10.3	172	53
2	CCN	11/30/2004	2.4	1.9	29.9	855	192
3	CCN	09/24/2008	2.4	1.9	69.4	164	17
4	CCN	09/11/2008	3.8	3.3	165.6	1411	213
5	Craig	06/22/2007	2.2	1.7	37.5	507	77
6	Creighton	02/07/2008	2.4	1.9	45.9	197	41
7	Creighton	03/14/2009	2.6	2.1	197.7	2933	627
8	Creighton	12/06/2008	2.9	2.4	25.3	161	54
9	Creighton	06/15/2007	3.0	2.5	27.6	591	402
10	Creighton	10/07/2007	3.1	2.6	53.6	801	408
11	Kidd Creek	03/02/2006	1.6	1.0	23.5	223	21

CCN Copper Cliff North Mine

M_n and $M_{w,m}$ are the main shock magnitudes of the sequence in Nuttli and moment magnitude, respectively, and t_N is the total duration of each sequence

1994; Hudyma and Potvin 2010; Estay 2014). For the single-link analysis, the proximity of two clusters is defined as the minimum distance between any two points in each cluster (Fig. 7). The same distance of $d \leq 50$ m was selected to separate clusters in space. It should be noted that this analysis does not restrict the spatial extent (volume) associated with the main event, i.e. the resulting seismicity is free to form chains of any size and shape.

Table 1 indicates the number of events in each sequence pre and post clustering.

3.3. Gutenberg–Richter and Modified Omori's Law Parameters

For each filtered and clustered aftershock sequence, the Gutenberg–Richter's b value and modified Omori's law parameters K, p and c are estimated by the maximum likelihood method (Vallejos and McKinnon 2009a, b, 2010; Vallejos 2010; Aki 1965; Ogata 1983).

The Gutenberg–Richter law is defined as

$$\log(N) = a - bM_w, \tag{5}$$

where N is the cumulative number of earthquakes with magnitudes equal or larger than M_w and parameters a and b are constants. In particular, the b value depends on the tectonic regimes (Schorlemmer et al. 2005) and the stress regime (Scholz 1968; Mikumo and Miyatake 1979; Mori and Abercrombie 1997; Enescu and Ito 2003).

The Gutenberg–Richter's b value is calculated as

$$b = \frac{\log(e)}{\bar{M}_w - M_{w,c} + \Delta M_{bin}/2}, \tag{6}$$

where $\bar{M}_w$ is the mean magnitude of events that $M_w \geq M_{w,c}$. ΔM_{bin} is the binning width of the catalogue. Each bin has a width of 0.1.

Concerning the MOL's parameters, given the occurrence times t_i ($i = 1, \ldots, N$) of the individual N events in a time interval $[T_A, T_B]$ the log-likelihood function of Eq. (1) can be expressed by

$$\ln L(K,p,c,T_A,T_B) = N\ln K - p\sum_{i=1}^{N}\ln(t_i + c) - KA(p,c,T_A,T_B), \tag{7}$$

where

$$A(p,c,T_A,T_B) = \begin{cases} \ln(T_B + c) - \ln(T_A + c) & p = 1 \\ [(T_B + c)^{1-p} - (T_A + c)^{1-p}]/(1-p) & p \neq 1 \end{cases}. \tag{8}$$

The maximum likelihood estimates (MLE) of the parameters K, p and c, are those values that maximize Eq. (7). The MOL parameters have been estimated into the complete duration of the sequence, i.e. $[T_A, T_B] = [t_0, t_N]$, where t_0 and t_N are the occurrence times of the main and last events in the clustered sequence, respectively.

3.4. Båth's Law

The empirical Båth's law (Richter 1958; Båth 1965) states that the average difference in magnitude

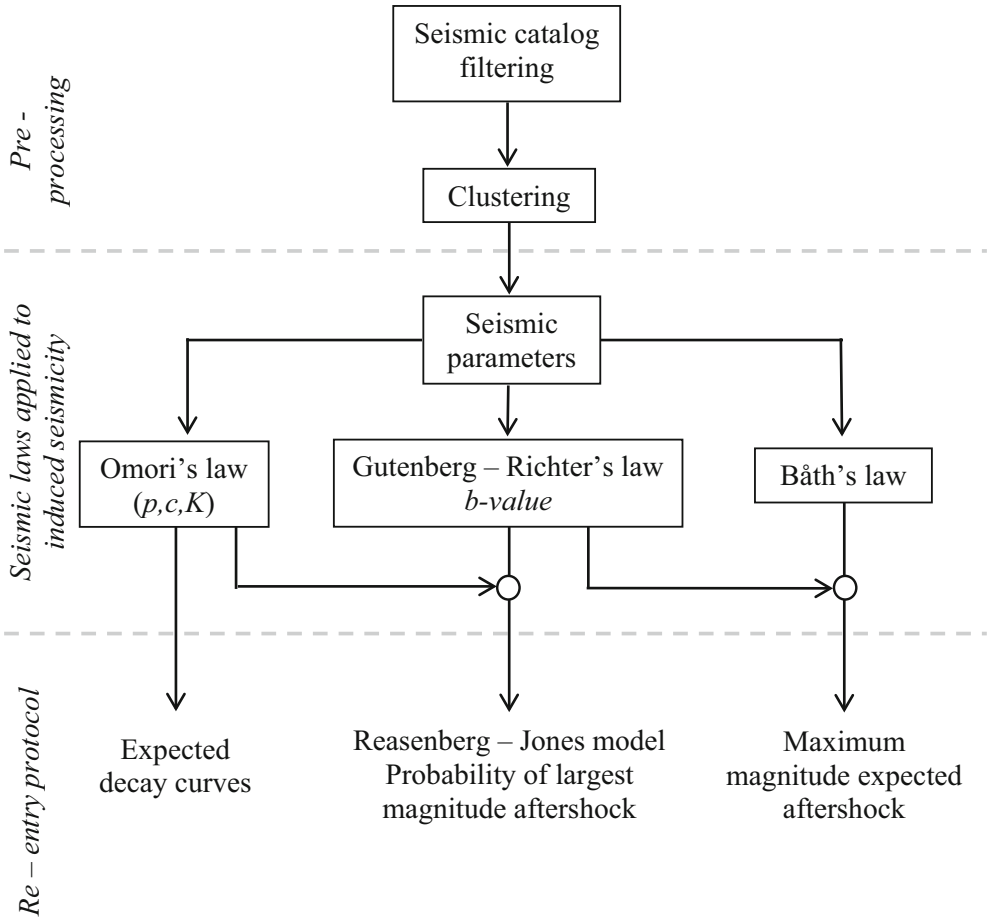

Figure 6
Methodology and results obtained in this paper

Table 2

Magnitude of completeness, $M_{w,c}$, for each sequence (Seq)

Seq	Site	$M_{w,c}$	R_{GoF} (%)
1	Copper Cliff North	− 1.4	87.7
2	Copper Cliff North	− 1.6	97.7
3	Copper Cliff North	− 1.7	91.8
4	Copper Cliff North	− 1.6	94.7
5	Craig	− 1.8	93.6
6	Creighton	− 1.5	92.2
7	Creighton	− 1.7	98.2
8	Creighton	− 1.5	93.0
9	Creighton	− 1.4	96.3
10	Creighton	− 1.4	94.2
11	Kidd Creek	− 2.0	90.2

R_{GoF} percentage of adjustment of each sequence applying the Goodness of Fit method

between a main shock and its largest aftershock in shallow earthquakes is constant and equal to 1.2 regardless of the main shock magnitude, i.e.

$$\Delta M_{\mathrm{w}} = M_{\mathrm{w,m}} - M_{\mathrm{w,LA}} \approx 1,2, \qquad (9)$$

where $M_{\mathrm{w,m}}$ and $M_{\mathrm{w,LA}}$ are the magnitudes of the main shock and the largest aftershock, respectively.

Several authors have applied and interpreted Båth's law to tectonic seismicity (Felzer et al. 2002; Console et al. 2003; Helmestetter and Sornette 2003; Shcherbakov and Turcotte 2004; Tsapanos 1990; Vere-Jones 1969), but few focus on induced seismicity (Vallejos and McKinnon 2009).

Shcherbakov and Turcotte (2004) proposes a modified Båth's law as follows:

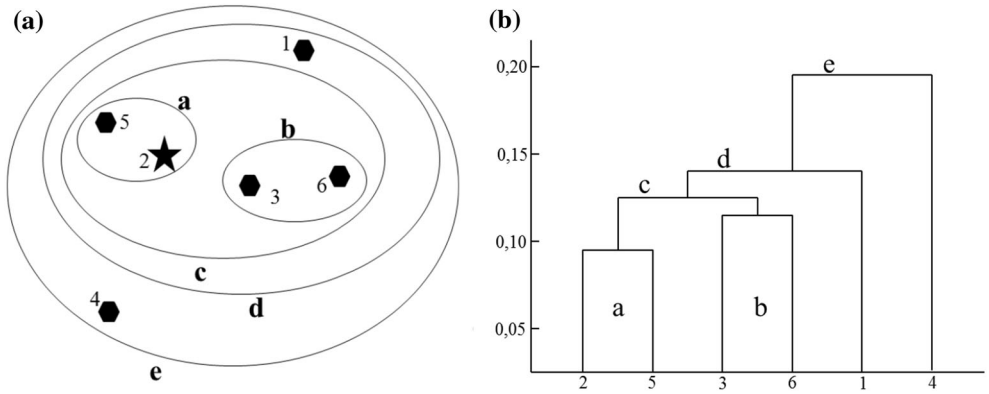

Figure 7
a Example of single-link clustering. The star represents the location of the main shock magnitude. **b** Dendrogram for single-link clustering

$$\Delta M_{\mathrm{w}}^{*} = M_{\mathrm{w,m}} - M_{\mathrm{w}}^{*}, \tag{10}$$

where M_{w}^{*} is the inferred largest aftershock estimated by Gutenberg–Richter's law, considering $N = 1$ in Eq. (5),

$$M_{\mathrm{w}}^{*} = \frac{a}{b}, \tag{11}$$

which is the value of the aftershock magnitude that was used in this study to evaluate the Reasenberg–Jones model, explained below.

3.5. Reasenberg–Jones Probability Model

The Reasenberg–Jones model (Reasenberg and Jones 1989, 1994) expresses the rate λ of aftershocks with magnitude M or larger, at time t following a main shock of magnitude $M_{\mathrm{w,m}}$ as follows:

$$\lambda(t, M_{\mathrm{w}}) = \frac{10^{a'+b(M_{\mathrm{w,m}}-M_{\mathrm{w}})}}{(t+c)^{p}}, \tag{12}$$

$$a' = \log(K) - b(M_{\mathrm{w,m}} - M_{\mathrm{w}}). \tag{13}$$

The probability, P, of one or more earthquakes occurring between magnitudes $M_{\mathrm{w},1}$ and $M_{\mathrm{w},2}$ in the time range $[t, t + \Delta t]$ is (Reasenberg and Jones 1989; Wiemer et al. 2002; Ford and Walter 2010)

$$P\left(M_{\mathrm{w},1} \le M < M_{\mathrm{w},2}; S \le t < T\right) = 1 - \exp\left(\int_{t}^{t+\Delta t} \lambda(t, M_{\mathrm{w}})\mathrm{d}t\right)_{M_{\mathrm{w},1}}^{M_{\mathrm{w},2}}. \tag{14}$$

A common error in calculating probability is that it integrates with respect to time and magnitude. The error arose from our incorrectly treating $\lambda(t,M_{\mathrm{w}})$ as a density function, when in fact it is a density with respect to t and a rate with respect to M (Reasenberg and Jones 1994).

Solving Eq. (14) results in

$$\begin{aligned} P &= 1 - \exp\left\{-\frac{(t+\Delta t+c)^{1-p} - (t+c)^{1-p}}{(1-p)}\left(10^{a'+b(M_{\mathrm{w,m}}-M_{\mathrm{w},1})} - 10^{a'+b(M_{\mathrm{w,m}}-M_{\mathrm{w},2})}\right)\right\} \quad \text{for} \quad p \neq 1 \\ P &= 1 - \exp\left\{-\ln\left(\frac{t+\Delta t+c}{t+c}\right)\left(10^{a'+b(M_{\mathrm{w,m}}-M_{\mathrm{w},1})} - 10^{a'+b(M_{\mathrm{w,m}}-M_{\mathrm{w},2})}\right)\right\} \quad \text{for} \quad p = 1 \end{aligned}, \tag{15}$$

where p and c are the modified Omori's law parameters, b is the Gutenberg–Richter's coefficient. a' can be expressed as

where $M_{\mathrm{w},2}$ is considered as the main shock magnitude, $M_{\mathrm{w,m}}$, $M_{\mathrm{w},1}$ is the largest aftershock magnitude, $M_{\mathrm{w,LA}}$ and Δt was considered as 1 h.

4. Results

In the following section, the statistical properties of mining-induced aftershock sequences and their implications for re-entry protocol development are presented. The scaling relations (modified Omori's law, Gutenberg–Richter and Båth's law) and a stochastic model (Reasenberg and Jones) are applied to several mining-induced aftershock sequences from different mine sites in Ontario, Canada.

4.1. Gutenberg–Richter

Figure 8 presents the frequency distribution of each sequence and its Gutenberg–Richter's adjustment. Figure 9 shows the b values from Gutenberg–Richter's law for each filtered and clustered sequence as a function of the main shock magnitude. The regression line for all the data is included in this figure. In general, there is no clear dependency of the b value on the main shock magnitude.

The b value has a mean of 1.39 ± 0.4. The mean value is within the ranges published by Wiemer et al. (2002) and Nuannin et al. (2002), for induced seismicity in South Africa and Sweden, respectively, but a little lower that those obtained for El Teniente Mine (Estay 2014). Variations of b values in induced seismicity can be explained by the high and low stress (Scholz 1968) (for low values of b, higher stress in the mine), thermal gradients (Warren and Latham 1970), and more recently, the effects of pore pressure in rock (Bachmann et al. 2012). Schorlemmer et al. (2005) also indicate that for tectonic seismic events (California and Japan), normal faulting events show the highest b values (1.07 ± 0.06), strike slip events show intermediate values (0.96 ± 0.1) and thrust events the lowest (0.77 ± 0.08).

However, when considering only the results for the Creighton mine, a value of $R^2 = 0.32$, indicating a better correlation between the parameter b and the magnitude of the main event.

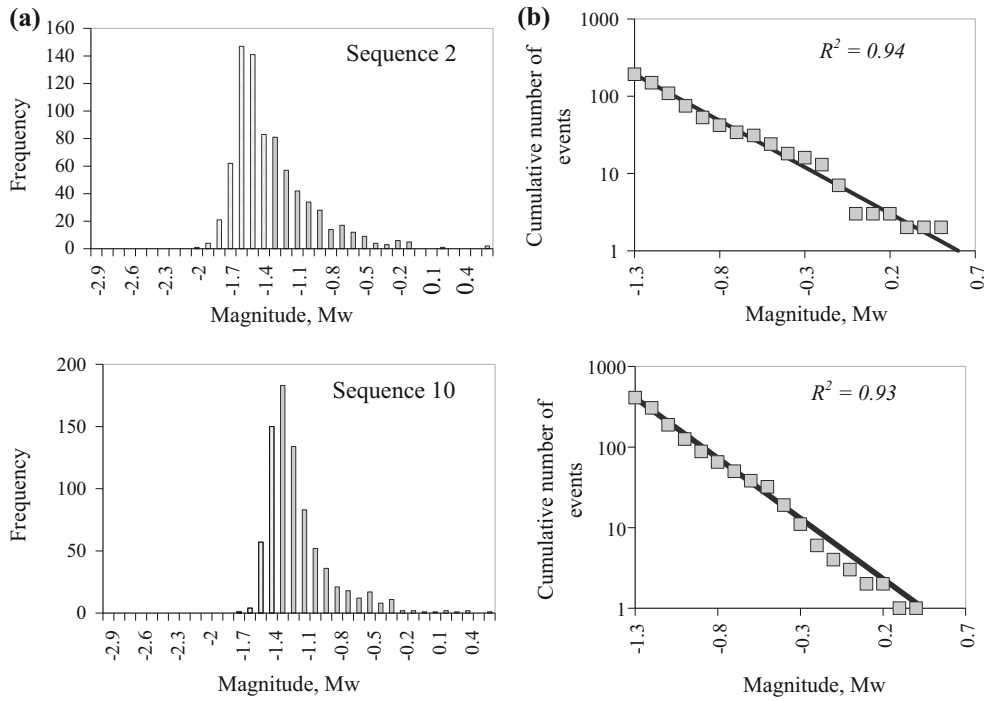

Figure 8
Some examples of **a** histogram of aftershock sequence before filtering. The striped bars correspond to those with M_w values lower than $M_{w,c} = -1.3$. **b** Frequency–magnitude distribution and its respective Gutenberg–Richter adjustment after filtering with the coefficient of adjustment, R^2

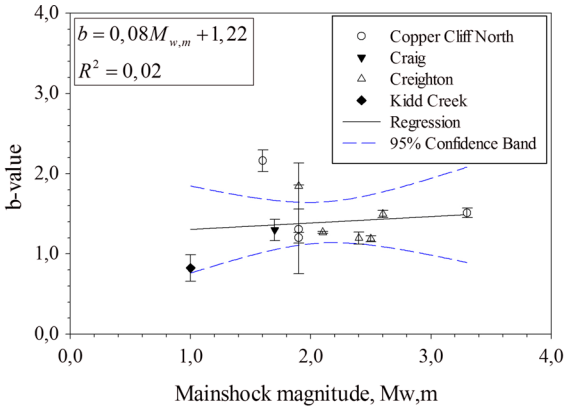

Figure 9
Dependence of b value on the main shock magnitude, $M_{w,m}$ for each filtered and clustered sequence. Errors bars correspond to the standard error proposed by Shi and Bolt (1982)

4.2. *Modified Omori's Law*

The modified Omori's law p value varies from sequence to sequence within range of 0.70–1.09, and an average of 0.83 ± 0.13, in accordance with the results obtained by Utsu et al. (1995), Wang (1994) and Nyffeneger and Frohlich 2000). Null correlation between p and the magnitude $M_{w,m}$ of the main event is found (Fig. 10a).

It is expected that for mining-induced aftershock sequences, the mechanism involved (e.g. pillar burst, fault slip, strain burst) may play a role in the aftershock productivity and the p value. Guo and Ogata (1997) have shown that p values depends if the events corresponds to intra-plate (1.15 ± 0.25) or inter-plate earthquakes (0.95 ± 0.10). On the other hand, Yamanaka and Shimazaki (1990) have shown that the aftershock productivity also depends on the seismic mechanism. The spread shown in Fig. 10a reflects the nature of the induced seismicity, suggesting that the seismicity mechanism may play a role in determining the speed of decay as it occurs in tectonic earthquakes.

As was done in Sect. 4.1 for the b value, considering only the values obtained for the Creighton mine, a high correlation between p and $M_{w,m}$ is obtained ($R^2 = 0.66$).

Figure 10b, c presents the correlations between the parameters K and c of the modified Omori's law (MOL) with the magnitude of the main event. Both parameters present significant positive correlations, with a value of the coefficient of adjustment R^2 equal to 0.49 and 0.59, respectively.

As expected, the K value increases as the main shock magnitude also increases. This is because the K value is an activity parameter related to the number of events within the sequence.

On the other hand, in tectonic analysis, the physical meaning of the c value is attributable to the complex feature of the rupture process (Yamakawa 1968) as a time shift that relates to the rate of aftershocks in the early part of the sequence (Enescu et al. 2009) that have smaller signal amplitudes and are not completely detected (Hamaguchi and Hasegawa 1970; Kagan and Houston 2005). Also, c value behaves as the constant which does not allow the Eq. (1) to be undefined at $t = 0$ (Narteau et al. 2002). This behaviour seems to be replicated by the c values in induced seismicity (Fig. 10c), which at higher magnitudes, present higher c values, thus there would be aftershocks in an early stage of the sequence that the monitoring system is unable to detect.

The values of the MOL's parameters are shown in Table 3.

4.3. *Båth's Law*

Table 4 shows the values of the main shock magnitude ($M_{w,m}$), the magnitude of the largest aftershock of each sequence ($M_{w,LA}$), the Gutenberg–Richter's parameters (a, b) and the difference ΔM_w and ΔM_w^* explained in Sect. 3.4.

A mean of $\Delta M_w = 2.1 \pm 0.6$ is obtained, which is clearly larger than the one proposed by Båth for tectonics seismicity. Table 4 also presents the results of applying Eq. (10) to the induced seismicity sequences. An average of $\Delta M_w^* = 1.5 \pm 0.6$ is obtained. This value is very close to the value proposed by Båth, which also, is a better result than the one obtained with ΔM_w.

4.4. *Reasenberg–Jones Model*

To estimate p, c, a' and b values for the Reasenberg–Jones model, the empirical tendencies obtained in Sects. 4.1 and 4.2 were used.

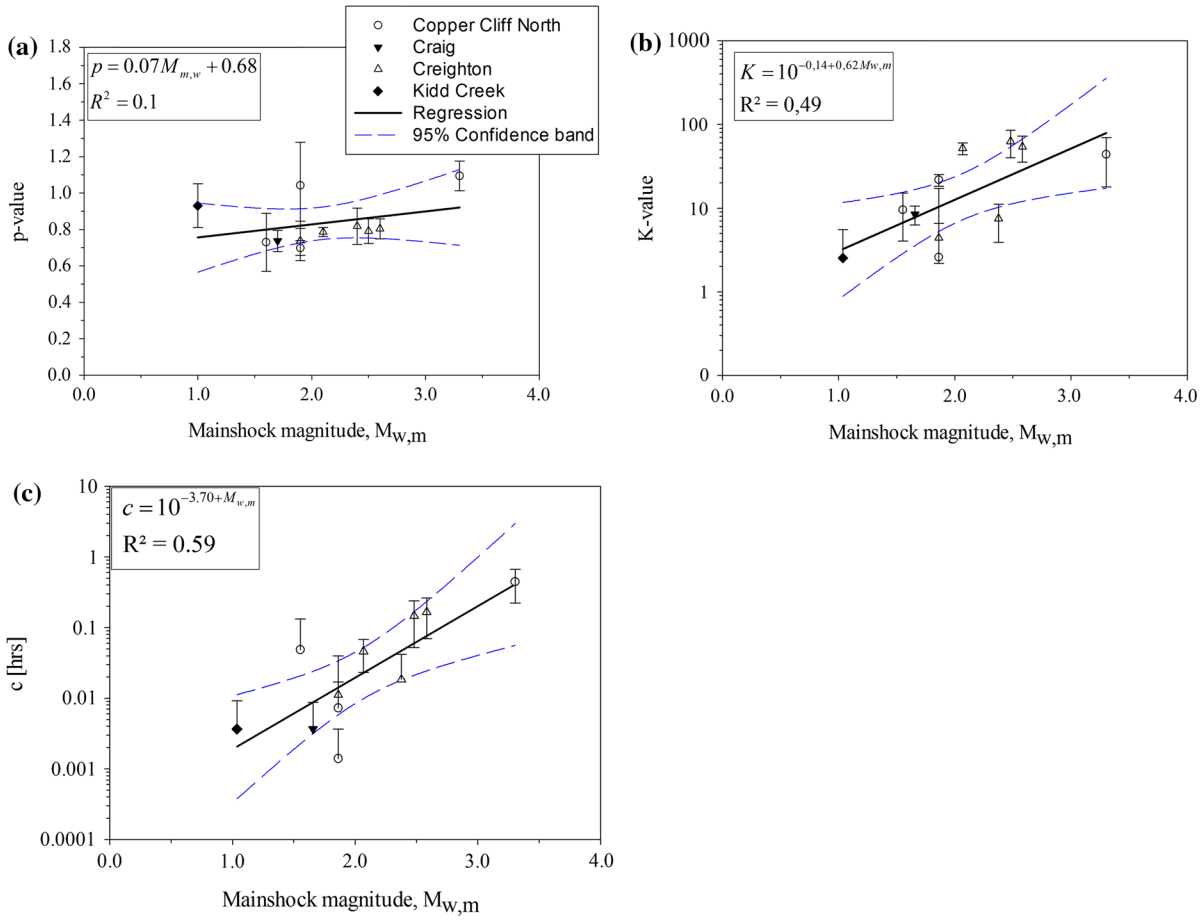

Figure 10
Dependence of the MOL parameters **a** p value, **b** K value and **c** c value with the main shock magnitude. The p and c error bars correspond to the uncertainty estimation from the MLE method. K error bars are estimated using the propagation of uncertainty

Table 3

MOL's parameters for each sequence (Seq)

Seq	Site	$M_{w,m}$	K	c	p
1	Copper Cliff North	1.6	9.54	0.05	0.73
2	Copper Cliff North	1.9	21.72	0.00	0.70
3	Copper Cliff North	1.9	2.60	0.01	1.04
4	Copper Cliff North	3.3	43.76	0.44	1.09
5	Craig	1.7	8.41	0.00	0.74
6	Creighton	1.9	4.39	0.01	0.74
7	Creighton	2.1	51.82	0.05	0.79
8	Creighton	2.4	7.50	0.02	0.82
9	Creighton	2.5	62.51	0.15	0.79
10	Creighton	2.6	54.03	0.17	0.80
11	Kidd Creek	1.0	2.53	0.00	0.93

Because the correlation obtained for the parameter p with $M_{w,m}$ is close to 0, we decided to use the mean value of $p = 0.83$.

The value of the parameter c was estimated using Eq. (16)

$$c = 10^{-3.70+\bar{M}_{w,m}} \tag{16}$$

where $\bar{M}_{w,m}$ is the average value of the main shock magnitudes of the sequences. Considering a $M_{w,c}$ value of -1.3, Eq. (16) can be expressed as

$$c = 10^{-2.50+(\bar{M}_{w,m}-M_{w,c})} \tag{17}$$

Furthermore, a' and b values were directly obtained from the equation presented in Fig. 10a, where K value is written as

Table 4

Results of converting Nuttli magnitude into moment magnitude applying Eq. (3) and the results of ΔM_w and its modified form, ΔM_w^*

Sequence	Site	$M_{w,m}$	$M_{w,LA}$	a	b	M_w^*	ΔM_w	ΔM_w^*
1	CCN	1.6	− 0.8	− 0.50	2.16	− 0.2	2.4	1.8
2	CCN	1.9	0.6	1.10	1.20	0.9	1.3	1.0
3	CCN	1.9	0.1	− 0.06	1.31	0.0	1.8	1.9
4	CCN	3.3	0.1	0.83	1.51	0.6	3.2	2.7
5	Craig	1.7	− 0.1	0.61	1.30	0.5	1.8	1.2
6	Creighton	1.9	− 0.8	− 0.25	1.85	− 0.1	2.7	2.0
7	Creighton	2.1	0.1	1.55	1.27	1.2	2.0	0.9
8	Creighton	2.4	− 0.3	0.56	1.20	0.5	2.7	1.9
9	Creighton	2.5	0.3	1.44	1.19	1.2	2.2	1.3
10	Creighton	2.6	0.4	1.13	1.50	0.8	2.2	1.8
11	Kidd Creek	1.0	− 0.2	0.49	0.83	0.6	1.2	0.4

CCN Copper Cliff North Mine

$$K = 10^{-0.14+0.62M_{w,m}}. \quad (18)$$

Considering a $M_{w,c}$ value equal to − 1.3, Eq. (18) can be written in function of the difference $M_{w,m} - M_{w,c}$ as

$$K = 10^{-0.95+0.62(M_{w,m}-M_{w,c})}. \quad (19)$$

This relation is associated to $10^{a'+b(M_{w,m}-M_w)}$ of Eq. (12), so $a' = -0.95$ and $b = 0.62$.

5. Re-entry Protocol Development

In this section, a space–time–magnitude re-entry protocol is proposed. The space and time that establishes the exclusion zone after a main shock were defined by an exclusion radius and the T_{MC} values. Also, the correlation between these values and the main shock magnitudes of each sequences is shown.

Seismic decay curves are estimated considering the MOL's parameters. These curves provide information on the decay patterns of an on-going sequence.

The Reasenberg–Jones probability of occurrence of the maximum expected magnitude is estimated using the results previously obtained with Gutenberg–Richter's law, Omori's law and Båth's law.

5.1. Exclusion Zone

The exclusion zone is defined as the volume around the main event's hypocentre for which access is restricted by the re-entry protocol. To provide some guidance on the possible exclusion zone size after large magnitude events, the spatial extent of the events was analysed. For simplicity purposes, this zone was represented by a sphere with radius R^*.

In some cases, the first event in the sequence was not necessarily associated with the cluster of seismicity. Considering this, the centre of the sphere will be the centroid of the seismicity that occurs during the first hour after the main shock. This point ensured a better statistical representation of the size of the affected zone, allowing a greater representativeness of the zone where the rupture begins. Three spherical radii for the exclusion zone were estimated: the best-fit radius (R_{min}), the sum of seismic moment radius (R_{ssm}) and the sequence radius (R_{seq}) (Fig. 11)

The best-fit spherical radius was estimated minimizing the quadratic difference between the

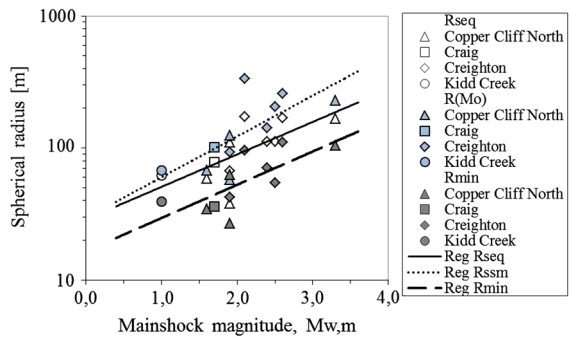

Figure 11
Spherical radii as functions of the main shock magnitude of the main event

Table 5

Regression equations and coefficient of adjustment (R^2) for each option of the exclusion zone radius

Methodology	Regression equation	R^2
Best spherical radius	$R_{\min} = 10^{1.22+0.25M_{w,m}}$	0.52
Sum of seismic moment radius	$R_{ssm} = 10^{1.47+0.31M_{w,m}}$	0.52
Sequence radius	$R_{seq} = 10^{1.46+0.25M_{w,m}}$	0.47

distances of the events belonging to the clustered sequence and the centroid of the exclusion zone. This allows including those events that could be generated and grouped in the edges of the rupture zone.

The sum of seismic moment radius was estimated considering the minimum radius that includes 90% of the total seismic moment of the sequence.

Finally, the sequence radius was estimated considering 90% of the events clustered in each sequence.

Figure 11 presents the resulting of the three spherical radii estimated as a function of the main shock moment magnitude for all the sequences analysed. Despite some natural spread in the data, a significant adjustment (Table 5) between the spherical radius and the magnitude of the main shock can be recognized.

So, for example, in case of a seismic event with $M_{w,m} = 2.0$, results in values of $R_{\min} = 53$ m, $R_{seq} = 89$ m and $R_{ssm} = 123$ m.

Moreover, in Ontario mines, depending on the type of rupture, different exclusion radii are used (Vallejos 2010)

$$\text{Source radius (SR)} = \begin{cases} < 50\,\text{m} & \text{Strain burst and entry mining methods} \\ 50 < \text{SR} < 100 & \text{Open stope mining} \\ > 100 & \text{Regional fault slip} \end{cases}.$$

With respect to the above given equation, the values proposed for the exclusion zone radius coincide with the source radius used in Ontario mines. In this regard, it is proposed to use the highest value between SR and the one obtained with the equations presented in Table 5, depending of the seismic mechanism.

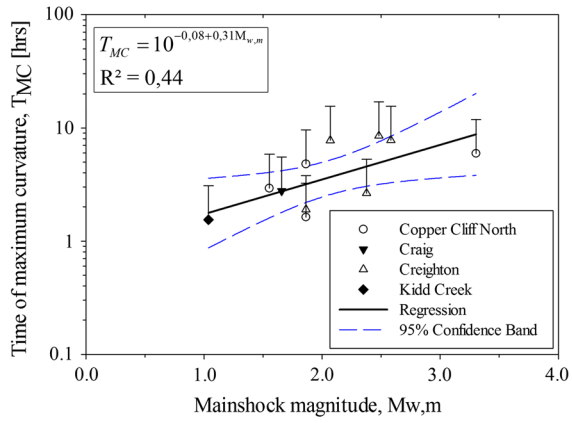

Figure 12
Correlation between the time of maximum curvature T_{MC} and the magnitude of the main event

5.2. Modified Omori's Law

Figure 12 presents the correlation between the time of maximum curvature (2) of the modified Omori's law and the magnitude of the main event. T_{MC} defines the transition between the highest to lowest rate change (Vallejos and McKinnon 2010) and is recommended as a preliminary estimate of the time at which it may be considered appropriate to re-enter an area affected by a large magnitude event (Vallejos and McKinnon 2008, 2010).

As expected, T_{MC} increases as $M_{w,m}$ increases too, related to a higher seismic activity and the longer time needed to reach the lowest event rate change. To develop a real time re-entry protocol, a series of average MOL curves are defined as a reference to evaluate the actual sequence.

For applying Eq. (1) to the number of events at time t occurring during the last time window Δt, it is necessary to consider its integral form for a time interval $[T_A, t]$, given by

$$N_{[t,T_A]} = \int_{T_A}^{t} n(t)\mathrm{d}t = \begin{cases} K \ln\left(\frac{t+c}{T_A+c}\right) & p = 1 \\ \frac{K}{1-p}\left[(t+c)^{1-p} - (T_A+c)^{1-p}\right] & p \neq 1 \end{cases} \quad (20)$$

by fixing the range of the time interval $[T_A, t]$ to a given time period Δt

$$t - T_A = \Delta t, \tag{21}$$

and substituting this expression in Eq. (20), the following is obtained:

$$N_{[t,t-\Delta t]} = \begin{cases} K \ln\left(\frac{t+c}{t-\Delta t+c}\right) & p = 1 \\ \frac{K}{1-p}\left[(t+c)^{1-p} - (t-\Delta t+c)^{1-p}\right] & p \neq 1 \end{cases} \tag{22}$$

that represents the number of events at time t occurring during the previous time window Δt. In this case, a value of $\Delta t = 1$ h is selected. The values of the parameters p, c and K were estimated as explained in Sect. 4.4.

The resulting seismic decay curves are used to provide information on the decay patterns of an ongoing sequence (Fig. 13). In addition, the time of maximum curvature T_{MC} (Eq. (2)), and the event rate at T_{MC} are incorporated into the chart. These parameters lead to evaluate a maximum curvature boundary in the event rate diagram that is used to estimate T_{MC} in real time, i.e. when the event rate crosses this boundary the maximum curvature has been reached (Fig. 13).

The dashed line in Fig. 13 corresponds to the decay curve of sequence 16, using its own values of p, c and K (see Table 3), which properly follow the actual sequence data. However, the difference between both curves (dashed line and continuous line with $M_{w,m} = 2.6$) is small, where the continuous curve slightly underestimates the actual decay curve. This underestimation results in a T_{MC} value variation from 5.3 (considering the continuous line) to 7.8 h (with the dashed line).

5.3. Reasenberg–Jones Model

In this section, an application of the Reasenberg–Jones model was made, considering the values of a', b, c and p explained in Sect. 4.4. Also, the $M_{w,m} - M_{w,1}$ (Eq. (15)) difference was considered as $M_{w,m} - M_w^*$.

As explained in Sect. 4.4, the dependences of Gutenberg–Richter and Omori's parameters with main shock magnitudes were used to plot the fitted Reasenberg–Jones probability curve line (Fig. 14). Also, this curve is compared with the curve proposed by Reasenberg and Jones (1989, 1994) and with those obtained for each sequence.

In Fig. 14, it can be observed how the curve associated to the methodology proposed by Reasenberg–Jones, (using the average values of the parameters of the aftershock sequences)

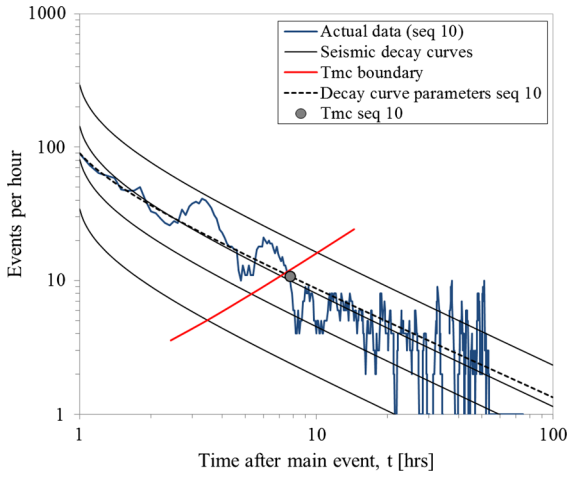

Figure 13
Events per hour as a function of time and magnitude after a main event applied to sequence 10 with $M_{w,m} = 2.6$. The dashed line corresponds to the decay curve calculated with the results obtained in Table 3 (sequence 10). The grey point indicates the value of the T_{MC} for sequence 10

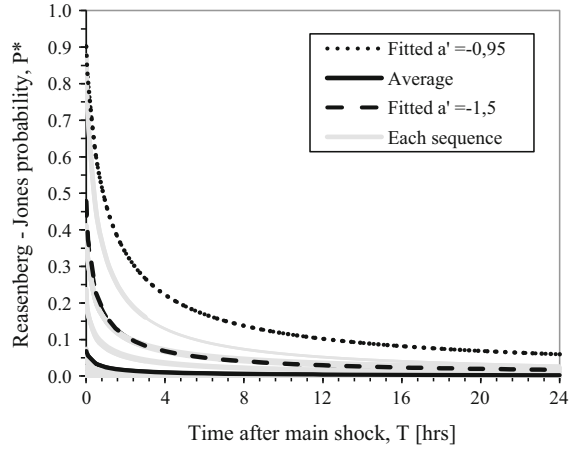

Figure 14
Application of Reasenberg–Jones probability model (Eq. (15)), considering the values of the parameters of each sequence (grey lines); the average value of the parameters as proposed by Reasenberg and Jones (1989, 1994) (continuous black line): $a' = -3.60$, $b = 1.39$, $c = 0.08$, $p = 0.83$; the values estimated using the methodology proposed in this study with $a' = -0.95$ (dotted line) and with $a' = -1.50$ (dashed line)

underestimates the results obtained in each one of the Ontario sequences.

On the other hand, the methodology proposed in this study overestimates these curves. This is mainly due to the value of a' (Eq. (13)), which greatly influences the behaviour of the probability curve, as shown in Fig. 14. In this case, considering the induced seismicity in Canada mines, the adjusted curve best represents the behaviour of the probability of occurrence of a seismic event with the magnitude that complies with the expected Bath law for each sequence ($\Delta M_w^* = 1.5$).

6. Discussion

For adjusting the parameter b of the Gutenberg–Richter's law, it is necessary first to confirm that the magnitude distribution can be explained by this scaling relation. Gibowicz and Kijko (1994) explained the bimodal distribution behaviour of the mine seismicity, associated to non -omogeneous major geologic features, where low and high energies are released by mining and residual tectonic stress accumulated in the rock mass, respectively. In this study, all aftershock sequences have a unimodal frequency–magnitude distribution, which can be correctly explained by the Gutenberg–Richter's law (Fig. 8).

The adjusted b values did not present any trend with the main shock magnitude (Fig. 9). The mines located in the SIC (Creighton, Craig and Copper Cliff North) have similar b values (except one sequence from Copper Cliff North). This may represent a particular type of faulting (normal, thrust or strike slip) and stress conditions in Ontario. Kid Creek mine presents a lower b value compared to the Ontario mines, which could indicate a local variation in the type of mechanism of mining-induced seismicity.

Linear relationships are adjusted to the MOL's parameters as a function of the main shock magnitude. The results presented low correlation values. This is considered as a first approximation to generalize the application of seismic parameters obtained from mining-induced seismicity. Using these relations is more representative to the seismic process generated by mining than using average values or values obtained from tectonic seismicity. The low correlation values can be improved by increasing the number of aftershock sequences used in the analysis.

For applying Båth's law to mining-induced aftershock sequences, it is necessary to consider the inferred largest aftershock obtained with the Gutenberg–Richter power law instead of the registered values. The mean value of this scaling relation is $\Delta M_w^* = 1.5 \pm 0.6$, however, ΔM_w^* differs from sequence to sequence with variation between 0.44 and 2.70.

7. Conclusions

Aftershocks are complex in nature. The statistics presented in the study are valuable in terms of the development and application of the re-entry protocol.

The correlations between Gutenberg–Richter's b value and the parameters of the modified Omori's law (MOL) with main shock magnitude, $M_{w,m}$, were explored. No significant correlations were obtained, except for the Omori's c and K values. The opposite occurs if only the results of Creighton mine are considered, where high correlations were obtained between b and p values with the magnitude of the main event. This high correlation may be related to the type of mechanism of the induced seismicity present in the mine. However, the number of sequences is not enough to establish final conclusions. Moreover, a conditional space–time exclusion zone based on the spherical radius (R^*), T_{MC}, and its correlation with $M_{w,m}$ have been proposed. Conditionality is obtained by setting the highest value between R^* and SR, depending of the mechanism of the induced seismicity.

A maximum expected aftershock magnitude was estimated applying a modified Båth's law, particular to Ontario aftershock sequences. A direct application of Båth's law to the induced seismicity data is not recommended. To obtain an uncorrelated value of ΔM_w with $M_{w,m}$, it is necessary to use an inferred largest aftershock, estimated by Gutenberg–Richter's law. Finally, a value of $\Delta M_w^* = 1.5$ was used in this study.

The concept of seismic decay curves was developed to provide information on the decay patterns of an on-going sequence. With this family of decay law

curves, it is possible to evaluate the path and decay pattern of an induced aftershock sequence after a large magnitude event. Also, considering the T_{MC}, it is possible to define a time after which it is safer to return to production in the affected area.

Finally, the Reasenberg–Jones probability model was applied to the seismic data, where the methodology proposed in this study presents results that are more in agreement with seismicity in Ontario than the methodology proposed by Reasenberg and Jones (1989, 1994).

Based on these main results, this study is a major development of re-entry protocols for mines, in which the space–time of the exclusion zone, the magnitude of the expected largest aftershock and its probability to occur were considered.

Acknowledgements

The re-entry protocol project was identified and supported by the MASHA Ground Control Committee (Mines and Aggregates Safety and Health Association) and funded by the WSIB (Workplace Safety and Insurance Board). The authors wish to acknowledge the permission of the mines to use their data and publish this work. We thank the reviewers for the helpful corrections that helped to improve this work. R.E. wants to thank Patricia Otaíza and Jorge Pascual for their assistance in correcting and translating the text.

References

Aki, K. (1965). Maximum likelihood estimate of b in the formula $\log N = a - bM$ and its confidence limits. *Bulletin of the Earthquake Research Institute, Tokyo, 43,* 237–239.

Bachmann, C., Wiemer, S., Goertz-Allmann, B., & Woessner, J. (2012). Influence of pore-pressure on the event-size distribution of induced earthquakes. *Geophysical Research Letters*. https://doi.org/10.1029/2012GL051480.

Båth, M. (1965). Lateral inhomogeneities in the upper mantle. *Tectonophysics, 2,* 483–514. https://doi.org/10.1016/0040-1951(65)90003-X.

Board, M., Brummer, R., & Seldom, S. (2001). Use of numerical modelling for mine design and evaluation. In W. A. Hustrulid & Bullock, R. L. (Eds.), *Underground mining methods: Engineering fundamentals and international case studies* (pp. 483–491). Littleton, Colorado: Society for Mining, Metallurgy and Exploration (SME).

Console, R., Lombardi, A. M., Murru, M., & Rhoades, D. (2003). Båth's law and the self-similarity of earthquakes. *Journal of Geophysical Research, 108*(B2), 2128–2136. https://doi.org/10.1029/2001JB001651.

Davis, S. D., & Frohlich, C. (1991a). Single-link cluster analysis, synthetic earthquake catalogues and aftershock identification. *Geophysical Journal International, 104,* 289–306. https://doi.org/10.1111/j.1365-246X.1991.tb02512.x.

Davis, S. D., & Frohlich, C. (1991b). Single-link cluster analysis of earthquake aftershocks: decay laws and regional variations. *Journal of Geophysical Research, 96,* 6335–6350. https://doi.org/10.1029/90JB02634.

Day, W. H. E., & Edelsbrunner, H. (1984). Efficient algorithms for agglomerative hierarchical clustering methods. *Journal of Classification, 1,* 7–24. https://doi.org/10.1007/BF01890115.

Dieterich, J. (1994). A constitutive law for rate of earthquake production and its application to earthquake clustering. *Journal of Geophysical Research, 99,* 2601–2618. https://doi.org/10.1029/93JB02581.

Enescu, B., & Ito, K. (2003). Values of *b* and *p*: their variations and relation to physical processes for earthquakes in Japan. *Annuals of Disaster Prevention Research Institute, Kyoto University*, *46B*, 709–719.

Enescu, B., Mori, J., Miyazawa, M., & Kano, Y. (2009). Omori–Utsu law *c*-values associated with recent moderate earthquakes in Japan. *Bulletin of the Seismological Society of America, 99*(2A), 884–891. https://doi.org/10.1785/0120080211.

Estay, R. (2014). *Metodología para la evaluación del desempeño de indicadores sísmicos en sismicidad inducida por la minería.* Msc thesis, Universidad de Chile

Felzer, K., Becker, T., Abercrombie, R., Ekström, G., & Rice, J. (2002). Triggering of the 1999 M_w 7.1 Hector Mine earthquake by aftershocks of the 1992 M_w 7.3 Landers earthquake. *Journal of Geophysical Research, 107*(B9), 2190–2202. https://doi.org/10.1029/2001JB000911.

Ford, S. R., & Walter, W. R. (2010). Aftershock characteristics as a means of discriminating explosions from earthquakes. *Bulletin of the Seismological Society of America, 100*(1), 364–376. https://doi.org/10.1785/0120080349.

Frohlich, C., & Davis, S. (1985). Identification of aftershocks of deep earthquakes by a new ratios method. *Geophysical Research Letters, 12*(10), 713–716. https://doi.org/10.1029/GL012i010p00713.

Frohlich, C., & Davis, S. D. (1990). Single-link cluster analysis as a method to evaluate spatial and temporal properties of earthquake catalogues. *Geophysical Journal International, 100,* 19–32. https://doi.org/10.1111/j.1365-246X.1990.tb04564.x.

Gibowicz, S., & Kijko, A. (1994). Bimodal distribution of mine tremors: An introduction. In An introduction to mining seismology (pp. 22–23). San Diego, California: Academic Press.

Gibson, H., Richardson, D., Hannington, M., Gibbins, S., DeWolfe, M., & Duff, D. (2003). The Kidd Creek volcanogenic massive sulphide deposit: A growing giant, after forty years of mining, exploration and research. In *Ore Deposits at depth conference, Keynote talk* (pp. 24–25). Ontario, Canada.

Guo, Z., & Ogata, Y. (1997). Statistical relations between the parameters of aftershocks in time, space, and magnitude. *Journal of Geophysical Research, 102*(B2), 2857–2873. https://doi.org/10.1029/96JB02946.

Hamaguchi, H., & Hasegawa, A. (1970). An investigation on the aftershocks of the Tokachi-oki earthquake of 1968, (2) Statistical

study on time distribution. *Science reports of the Tohoku University. Series 5, Geophysics, 20*(3), 119–133.

Hartigan, J. A. (1975). *Clustering algorithms (probability & mathematical statistics)*. New York: John Wiley & Sons Inc.

Helmestetter, A., & Sornette, D. (2003). Båth's law derived from the Gutenberg–Richter law and from aftershock properties. *Geophysical Research Letters, 30*(20), 2069–2072. https://doi.org/10.1029/2003GL018186.

Hudyma, M., & Potvin, Y. (2010). An engineering approach to seismic risk management in hard rock mines. *Rock Mechanics and Rock Engineering, 43,* 891–906. https://doi.org/10.1007/s00603-009-0070-0.

Ito, K., & Matsuzaki, M. (1990). Earthquakes as self-organized critical phenomena. *Journal of Geophysical Research, 95,* 6853–6860. https://doi.org/10.1029/JB094iB11p15635.

Kagan, Y., & Houston, H. (2005). Relation between main shock rupture process and Omori's law for aftershock moment release rate. *Geophysical Journal International, 163,* 1039–1048. https://doi.org/10.1111/j.1365-246X.2005.02772.x.

Ling, R. F. (1973). A probability theory of cluster analysis. *Journal of American Statistical Association, 68,* 159–196. https://doi.org/10.2307/2284161.

Malek, F., Suorineni, F.T. & Vasak, P. (2009). Geomechanics strategies for rockburst management at Vale Inco Creighton Mine. In M. Diederichs & Grasselli, G. (Eds.), *Rock engineering in difficult conditions*, proceedings of the 3rd CANUS rock mechanics symposium, Toronto, Canada.

McQuitty, L. L. (1957). Elementary linkage analysis for isolating orthogonal and oblique types and typal relevancies. *Educational and Psychological Measurement, 17,* 207–229.

Mikumo, T., & Miyatake, T. (1979). Earthquake sequences on a frictional fault model with non-uniform strengths and relaxation times. *Geophysical Journal of the Royal Astronomical Society, 59,* 497–522. https://doi.org/10.1111/j.1365-246X.1979.tb02569.x.

Mori, J., & Abercrombie, R. (1997). Depth dependence of earthquake frequency-magnitude distribution in California: implications for rupture initiation. *Journal of Geophysical Research, 102*(B7), 15081–15090. https://doi.org/10.1029/97JB01356.

Mukwakwami, J., Lfrance, B., & Lesher, C. (2011). Back-thrusting and overturning of the southern margin of the 1,85 Ga Sudbury Igneous Complex at the Garson mine, Sudbury, Ontario. *Precambrian Research, 196–197,* 81–105. https://doi.org/10.1016/j.precamres.2011.10.020.

Narteau, C., Shebalin, P., & Holschneider, M. (2002). Temporal limits of the power law aftershock decay rate. *Journal of Geophysical Research, 107*(B12), 2359–2372. https://doi.org/10.1029/2002JB001868.

Natural Resources Canada and Ontario Geological Survey (2015). Copper Cliff, Greater Sudbury: A driving tour of Greater Sudbury's mining industry; GeoTours Northern Ontario series.

Nuannin, P., Kulhanek, O., Persson, L., & Tillman, K. (2002). Forecasting of increasing induced seismicity in the Zinkgruvan mine, Sweden, by using temporal variations of *b*-values. *Acta Montana, Series A, 21,* 13–25.

Nuttli, O. W. (1973). Seismic wave attenuation and magnitude relations for Eastern North America. *Journal of Geophysical Research, 78,* 876–885. https://doi.org/10.1029/JB078i005p00876.

Nyffeneger, P., & Frohlich, C. (2000). Aftershock occurrence rate decay properties for intermediate and deep earthquake sequences. *Geophysical Research Letters, 27*(8), 1215–1218. https://doi.org/10.1029/1998GL010371.

Ogata, Y. (1983). Estimation of the parameters in the modified Omori formula for aftershock frequencies by the maximum likelihood procedure. *Journal of Physics of the Earth, 31,* 115–124. https://doi.org/10.4294/jpe1952.31.115.

Reasenberg, P., & Jones, L. (1989). Earthquake hazard after a main shock in California. *Science, 24,* 1173–1176. https://doi.org/10.1126/science.243.4895.1173.

Reasenberg, P., & Jones, L. (1994). Earthquake aftershocks: Update. *Science, 265,* 1251–1252. https://doi.org/10.1126/science.265.5176.1251.

Richter, C. F. (1958). *Elementary seismology*. San Francisco: Freeman.

Scholz, C. H. (1968). The frequency-magnitude relation of microfracturing in rock and its relation to earthquakes. *Bulletin of the Seismological Society of America, 58*(1), 399–415.

Schorlemmer, D., Wiemer, S., & Wyss, M. (2005). Variations in earthquake-size distribution across different stress regimes. *Nature Letters, 437,* 539–542. doi:10.1038/nature04094

Shcherbakov, R., & Turcotte, D. (2004). A modified form of Båth's law. *Bulletin of the Seismological Society of America, 94,* 1968–1975. https://doi.org/10.1785/012003162.

Shi, Y., & Bolt, B. (1982). The standard error of the magnitude–frequency *b* value. *Bulletin of the Seismological Society of America, 72*(5), 1677–1687.

Sneath, P. H. A. (1957). The application of computers to taxonomy. *Journal of General Microbiology, 17,* 201–226. https://doi.org/10.1099/00221287-17-1-201.

Sonley, E., & Atkinson, G. M. (2005). Empirical relationship between moment magnitude and Nuttli magnitude for small-magnitude earthquakes in south-eastern Canada. *Seismological Research Letters, 76,* 752–755. https://doi.org/10.1785/gssrl.76.6.752.

Therriault, A., Fowler, A., & Grieve, R. (2002). The Sudbury Igneous Complex: A differentiated impact melt sheet. *Economic Geology, 97*(7), 1521–1540. https://doi.org/10.2113/gsecongeo.97.7.1521.

Tsapanos, T. (1990). Spatial distribution of the difference between the magnitudes of the main shock and the largest aftershock in the circum-pacific belt. *Bulletin of the Seismological Society of America, 80,* 1180–1189.

Utsu, T., Ogata, Y., & Matsu'ura, R. (1995). The centenary of the Omori formula for a decay law of aftershock activity. *Journal of Physics of the Earth, 43,* 1–33. https://doi.org/10.4294/jpe1952.43.1.

Vallejos, J.A. (2010). *Analysis of seismicity in mines and development of re-entry protocols*. PhD thesis, Queen's University, Canada.

Vallejos, J.A., & McKinnon, S.D. (2008). Guidelines for development of re-entry protocols in seismically active mines. In *Proceeding of the 42nd US Rock Mechanics Symposium*, San Francisco, California, ARMA/USRMS.

Vallejos, J.A., & McKinnon, S.D. (2009). Re-entry protocols for seismically active mines using statistical analysis of aftershock sequences. Rock engineering in difficult conditions. In *Proceedings of the 3rd CANUS Rock Mechanics Symposium*, Toronto, Canada.

Vallejos, J. A., & McKinnon, S.D. (2009). Scaling laws and their implications for re-entry protocol development. In *The 7th International Symposium on Rockburst and Seismicity in Mines*, Dalian, China.

Vallejos, J. A., & McKinnon, S. D. (2010). Omori's law applied to mining-induced seismicity and re-entry protocol development. *Pure and Applied Geophysics, 167,* 91–106. https://doi.org/10.1007/s00024-009-0010-7.

Vallejos, J. A., & McKinnon, S. D. (2011). Correlations between mining and seismicity for re-entry protocol development. *International Journal of Rock Mechanics and Mining Sciences, 48,* 616–625. https://doi.org/10.1016/j.ijrmms.2011.02.014.

Vere-Jones, D. (1969). A note on the statistical interpretation of Båth's law. *Bulletin of the Seismological Society of America, 59,* 1535–1541.

Villaescusa, E., Simser, B., & Carlisle, S. (2007). Stress measurements at great depth at Craig–Onaping Mines, Sudbury, Canada. Rock engineering in difficult conditions. In *Proceedings of the 3rd CANUS Rock Mechanics Symposium*, Toronto, Canada.

Wang, J.-H. (1994). On the correlation of observed Gutenberg–Richter's *b* value and Omori's *p* value for aftershocks. *Bulletin of the Seismological Society of America, 84,* 2008–2011.

Warren, N., & Latham, G. (1970). An experiment study of thermal induced microfracturing and its relation to volcanic seismicity. *Journal of Geophysical Research, 75,* 4455–4464. https://doi.org/10.1029/JB075i023p04455.

Wiemer, S., Gerstenberger, M., & Hauksson, E. (2002). Properties of the aftershock sequence of the 1999 M_w 7,1 Hector Mine earthquake: Implications for aftershock hazard. *Bulletin of the Seismological Society of America, 92*(4), 1227–1240.

Wiemer, S., & Wyss, M. (2000). Minimum magnitude of complete reporting in earthquake catalogues: Examples from Alaska, the Western United States, and Japan. *Bulletin of the Seismological Society of America, 90,* 859–869. https://doi.org/10.1785/0119990114.

Yamakawa, N. (1968). Foreshocks, aftershocks and earthquakes swarms (IV)—Frequency decrease of aftershocks in its initial and later stages. *Papers in Meteorology and Geophysics, 19,* 109–119.

Yamanaka, Y., & Shimazaki, K. (1990). Scaling relationship between the number of aftershocks and the size of the main shock. *Journal of Physics of the Earth, 38,* 305–324. https://doi.org/10.4294/jpe1952.38.305.

(Received April 19, 2016, revised October 21, 2017, accepted October 25, 2017, Published online November 1, 2017)